Complex electron-phonon driven lattice dynamics in ultrasmall-radius (5,0) carbon nanotubes

K.-P. Bohnen and R. Heid
Forschungszentrum Karlsruhe, Institut für Festkörperphysik, P.O. Box 3640, D-76021 Karlsruhe, Germany

C. T. Chan
Department of Physics and Institute for Nano Science and Technology, Hong Kong University of Science and Technology, Clear Water Bay, Hong Kong, China

(Received 10 December 2007; revised manuscript received 16 April 2008; published 4 June 2008)

By using first principles density functional perturbation theory, we computed the phonon dispersions of 4 nm diameter (5,0) carbon nanotubes. We investigated the development of phonon anomalies as the Fermi surface sharpens. The soft modes are related to the nesting features in the electronic band structure. We found that two phonon branches are strongly renormalized by electron-phonon coupling, and the anomaly of one phonon branch is traced to interband coupling while the anomaly of another phonon branch is due to intraband coupling. The complex behavior is explained using a simple model.

DOI: 10.1103/PhysRevB.77.235407 PACS number(s): 65.80.+n, 63.22.−m, 63.20.kd, 71.15.Mb

I. INTRODUCTION

Recently, ultrasmall radius single wall carbon nanotubes (SWNT) have been fabricated with a template method.[1] The small radius SWNTs are grown inside the channels of AlPO4–5 zeolite crystals. Since the channels have very small diameters, only SWNTs of 0.4 nm can form. Three types of SWNTs, namely (3,3), (4,2), and (5,0), are found inside the zeolite channels. The (3,3) and (5,0) tubes are predicted to be metallic by local density functional calculations.[2] These ultrasmall SWNTs are of special interest since they are very close to a one-dimensional (1D) system. In particular, they can serve as excellent prototypical systems to study electron-phonon (el-ph) interactions and the phenomenon of Peierls transition. For the (3,3) tube, a phonon branch was found to go soft at $q=2k_F$ at about room temperature.[3,4] The (5,0) tube was found to spontaneously distort when the atoms are relaxed in calculations that considered a primitive unit cell that contains 20 atoms.[4] A detailed study of the lattice dynamics of the (5,0) tube, however, has not been done so far apart from a tight-binding investigation,[5] which, however, is a nonself-consistent approach and has been shown to give significantly different results from the fully self-consistent treatment in the case of the (3,3) tube.[3,4]

In this paper, we investigate the lattice dynamics of the (5,0) tube using density functional perturbation theory. We found rather complex and interesting phenomena due to el-ph coupling. The salient features of numerical results can be explained by a simple model.

The phonon anomalies for (5,0) are considerably more complex than what we have found for the (3,3) tube,[3] due to the more complex electronic structure of (5,0) near the Fermi level. The comparison of the el-ph interactions between (3,3) and (5,0) is in fact an interesting example of quantum size effects. In many situations, quantum size effects are direct consequences of the small size of the nano-object. The (3,3) and (5,0) have nearly the same radius, and there is thus no difference in the size. However, the el-ph interaction and phonon anomalies are entirely different since different ways of zone-folding lead to very different electronic structure, which in turn leads to a very different el-ph coupling. The quantum size effect here manifests itself as a boundary condition effect rather than a simple "size" effect.

II. METHOD

In this paper, we study the lattice dynamics and the phonon softening of (5,0) nanotubes using modern *ab initio* methods. Calculation of electronic properties are done by employing the well established density functional method. Phonon properties are obtained by determining the response of the electronic system to small changes in the atomic positions. This is done most efficiently by using a formulation that is known under the name of density functional perturbation theory (DFPT).[6] The DFPT approach gives complete phonon dispersion curves. Such an approach is very useful for the present studies, as the Kohn anomalies can occur at phonon wave vectors that may be incommensurate with the lattice, making supercell type calculations impractical. Our results are calculated with a "mixed-basis code,"[7] which employs plane waves up to a cutoff of 20 Ry, augmented by localized $2s$ and $2p$ functions. We employed Hamann–Schlüter–Chiang type of norm-conserving pseudopotentials,[8] which yields excellent results for carbon. Our DFPT is implemented within our mixed-basis code,[9] which has been applied successfully to describe the phonon dispersions and the electron-phonon coupling of many systems, including graphitic structures and nanotubes.

We used a supercell geometry in which the (5,0) nanotubes are arranged in a hexagonal array, with a nearest wall to wall distance of 10 Å. The tube-tube interactions are very small at such a distance, so the results represent the properties of an isolated tube. The primitive unit cell has 20 carbon atoms. The Fermi surface smearing is handled with a Gaussian broadening approach.[10] A Gaussian broadening width of 0.2 eV and 32 k points in the Brillouin zone are used for atomic coordinate relaxations. For phonon calculations, we employed a one-dimensional grid of 256 k points, and various Gaussian widths are employed in smearing the Fermi level, as explained below.

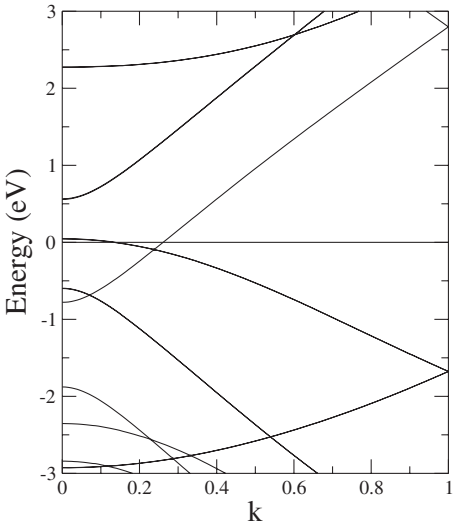

FIG. 1. Band structure of (5,0) for the atomic coordinates relaxed with a Gaussian width of 0.2 eV and 32 k points in the Brillouin zone. k is given in units of π/a. The Fermi energy is set to 0.

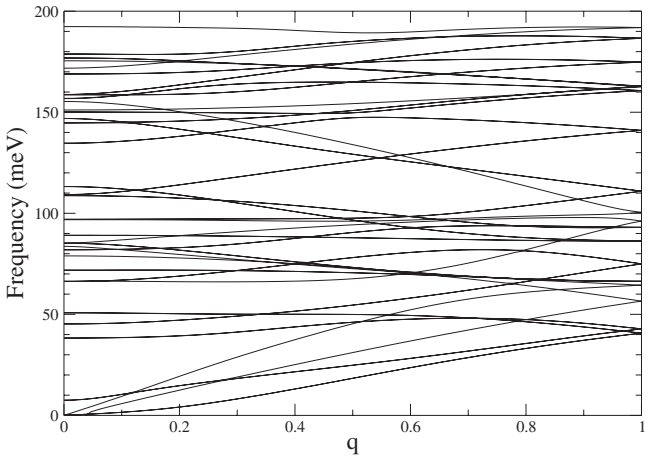

FIG. 2. Phonon dispersions of (5,0) calculated with a Fermi surface smearing of $w=0.2$ eV.

III. RESULTS

A. Electronic structure

Although the simple zone-folding picture predicts that the (5,0) tube is semiconducting, (5,0) is actually found to be a metal from LDA calculations. Due to $\sigma-\pi$ coupling induced by curvature effects, a nondegenerate band is pushed down in energy and becomes partially occupied. This is a consequence of the strong curvature effect due to the small radius of the (5,0) tube. The details of such an effect on the band structure of zigzag tubes had been discussed and explained by several authors.[2,11] This curvature effect has important consequences on the properties of small-diameter zigzag tubes. First of all, all (n,0) tubes with $n<7$ become metallic. This effect also causes small diameter zigzag tubes to have significantly higher work functions than graphite and (n,n) tubes.[12] For our particular case of (5,0), the tube is metallic because of this effect. Although the LDA band structure of the (5,0) tube can be found in the literature,[2] we show our calculated bands in Fig. 1 to facilitate the discussion of electron-phonon coupling in the following sections. Typical for this tube is the fairly high density of states at E_F of 0.35 states/(eV atom). This value is in good agreement with the value given in Ref. 13, especially in view of its high sensitivity to the k-point sampling and level broadening.

From Fig. 1, we see that a doubly degenerate negative effective mass band and one singly degenerate positive effective mass band cross the Fermi level. The Fermi points corresponding to the negative effective mass band and the positive effective mass band will be labeled as k_- and k_+, respectively. From Fig. 1, we found that (in units of π/a, i.e., zone−boundary=1 unit) the negative mass bands cross E_f at $k_-=0.13\pi/a$, while the positive mass band crosses E_f at $k_+=0.26\pi/a$.

As we shall see, the electronic structure of (5,0) gives rather unusual phonon properties for the (5,0) as a consequence of el-ph coupling. For the armchair (3,3), which has nearly the same radius, the band structure of (3,3) is qualitatively similar to the zone-folded graphene, although the Fermi point is at a slightly displaced k vector due to curvature. The phonon anomalies of (3,3) due to el-ph coupling are derived from the $q=0$ and $q=K$ (where K is the K point in the Brillouin zone of graphene) anomalies of graphene.[14] The (3,3) phonon anomalies can thus be qualitatively discussed by knowing the properties of graphene. For (5,0), the curvature effect changes the electronic band qualitatively near the Fermi level so drastically that it is not possible to discuss or understand the phonon anomalies from the electronic structure of graphene. In fact, within a zone-folding description, (5,0) has a gap and there is no phonon anomaly to worry about.

B. Phonon dispersion

In 1D systems, we have diverging susceptibilities at the nesting vector q's that connect Fermi points that have slopes of opposite signs on either side of the q-vector. By examining the band structure of the (5,0) tube, we expect strong el-ph coupling, and thus phonon anomalies at (i) $q=2k_-=0.26\pi/a$, (ii) $q=2k_+=0.52\pi/a$, and (iii) $q=k_+—k_-=0.13\pi/a$. The details of the phonon anomalies depend on the el-ph coupling strength and the density of states.

The phonon dispersions calculated using the first principles approach with a series of Gaussian broadening width (w), including $w=0.2$, 0.1, and 0.025 eV, are shown in Figs. 2–4 respectively. In Fig. 3 ($w=0.1$ eV) and Fig. 4 ($w=0.025$ eV), we plot only those symmetry class corresponding to phonon branches that the el-ph coupling has a visible renormalization of the phonon frequencies. From these figures, we can observe the development of phonon anomalies and soft modes as the Fermi surface sharpens. In Fig. 4, we use arrows to indicate the q vectors identified above to highlight the relationship between the nesting q vectors and the phonon anomalies. For all these phonon calculations, the atomic coordinates are obtained by relaxing the system with a Gaussian width of 0.2 eV. As we can see from Fig. 2, the phonons are not soft at that broadening. As the Fermi surface

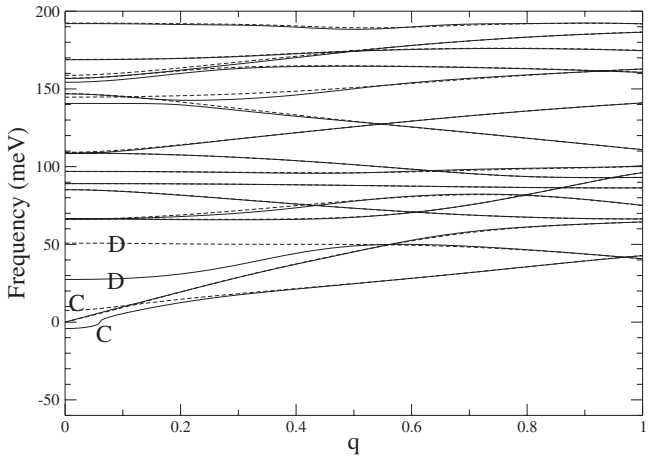

FIG. 3. Phonon dispersions of (5,0) calculated with a Fermi surface smearing of $w=0.1$ eV are shown as solid lines. The dotted lines show the phonons calculated with $w=0.2$ eV for comparison. Only those modes that are noticeably affected by el-ph coupling are shown.

sampling sharpens at a Gaussian width of 0.025 eV, phonon anomalies are clearly identified and soft modes appear near $q=0.13\pi/a$ and $q=0.26\pi/a$. The $q=0.26\pi/a$ anomaly, due to intraband coupling of the doubly degenerate band, is considerably stronger than the interband $q=0.13\pi/a$ coupling, presumably because the doubly degenerate bands have a higher density of state near E_f. We do not find noticeable anomalies at $q=0.52\pi/a$ that can potentially occur due to interband coupling of the positive mass band crossing the Fermi level. The positive mass band has low density of states at E_f.

From Fig. 2, we see that with a Gaussian width of $w=0.2$, the phonon dispersions show no anomalies that are visible to the eye. We will focus on the low frequency modes. There are four acoustic modes that have frequencies

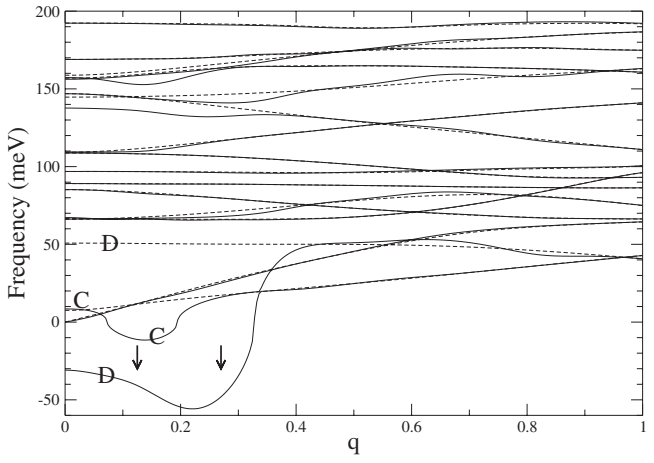

FIG. 4. Phonon dispersions of (5,0) calculated with a Fermi surface smearing of $w=0.025$ eV are shown as solid lines. The dotted lines show the phonons calculated with $w=0.2$ eV for comparison. Only those modes that are noticeably affected by el-ph coupling are shown. The arrows mark the nesting q vectors corresponding to $q=k_+—k_-=0.13$ and $q=2k_-=0.26$.

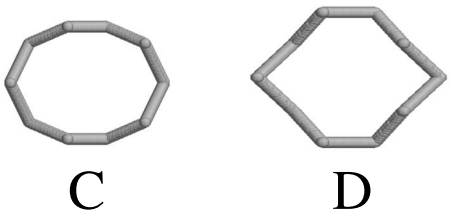

FIG. 5. Atomic distortions corresponding to the eigenvectors of the modes at the zone center for the branches labeled as C and D in Fig. 4.

that go to zero as $q\rightarrow 0$. The lowest frequency branch is doubly degenerate and corresponds to transverse vibration modes. Close to the Brillouin zone center, its frequency shows a quadratic dependence on q in agreement with predictions from continuum models.[15] The next branch corresponds to the twisting mode, which is a signature mode of the nanotubes, and the highest frequency acoustic branch is the longitudinal mode. We remark that the twisting mode actually has a small imaginary frequency at the zone center, which is found to be nearly independent of the Gaussian broadening width or the k-point sampling. This numerical artifact is traced to a small coupling between the tubes in different unit cells. There is actually a particular angle that the tube and its images have lower interaction energy due to intertube coupling, and that manifests as a small imaginary frequency for the "rotation" of the tube. This small intertube coupling does not affect our consideration of phonon anomalies due to el-ph coupling.

There are two modes that are of special interest and they are labeled as C and D in Figs. 3 and 4. The displacement eigenvectors for these two branches at $q=0$ are plotted in Fig. 5. At $q=0$, the phonon branches C and D have frequencies of about 7.5 and 50.8 meV, respectively, at $w=0.2$.

At a reduced Gaussian width of 0.1 eV, we found that the four acoustic phonon branches are hardly affected, but we see from Fig. 3 that the branches C and D are strongly renormalized near the zone center. Branch C becomes soft near the zone center, and branch D drops to below 30 meV.

If we further reduce the Gaussian width to 0.025 eV, the phonon anomalies are fully developed and the dips can be identified with the nesting q vectors at $q=0.13\pi/a$ and $0.26\pi/a$, respectively. Some interesting features are worth our attention. First, the branch C is driven unstable by the interband coupling between the negative mass bands and the singly degenerate positive mass band, which has a nesting $q=0.13\pi/a$. We note from Fig. 3 that this branch is soft at and near $q=0$ (not at $q=0.13\pi/a$) when the Gaussian width is 0.1 eV. At a smaller broadening of 0.025 eV, the frequency becomes finite again at $q=0$ and its vicinity, and the mode is soft near $q=0.13\pi/a$. Such an evolution, which involves a re-entrant stability of the mode at zone center (the mode first goes soft but becomes stable again), will be discussed in detail below. The branch D, which is still stable at $w=0.1$ eV, becomes now the dominant soft mode, and the mode is soft for a whole range of q vectors around $q=0.26\pi/a$ and extends all the way to the zone center. The mode is "softest" near the expected $q=0.26\pi/a$.

C. Frozen phonon calculations

The phonon dispersions give us useful information about the lattice dynamics of the system. However, these results correspond to the lowest order expansion of the Hamiltonian near the equilibrium. In order to explore the energy landscape for larger displacements near the equilibrium positions, we performed frozen phonon calculations. We first obtained the phonon eigenvectors for the phonon branches C and D at the zone center with $w=0.2$, where all phonons are stiff. We then distort the lattice according to frozen phonon displacements so that the atomic positions become $\mathbf{R}_i' = \mathbf{R}_i + \alpha \mathbf{P}_{i,\lambda}$, where the $\mathbf{R}_i'$ is the atomic coordinate of the tube at the zero-force position and $\mathbf{P}_{i,\lambda}$ is the atomic displacement at the i^{th} atom corresponding to the normalized eigenvector of the λ^{th} phonon mode. We will focus on the modes C or D at $k=0$. The atomic displacements that correspond to the phonon modes C and D at the zone center are shown in Fig. 5. The constant α is a scaling factor that controls the magnitude of the frozen phonon displacement.

The results shown in Fig. 6 are the relative energy change as the nanotube is distorted according to frozen phonon displacements. The energy changes in Fig. 6(a) are calculated with a Fermi surface smearing $w=0.1$ eV. Dots correspond to the frozen phonon displacement of mode C, while squares correspond to the frozen phonon displacement of mode D. The lines are fourth order polynomial fits to the calculated results. We see that both the energy change of the C and the D modes can be fitted very well with fourth order polynomials. The energy change corresponding to the D mode displacement is positive, consistent with the results shown in Fig. 3 that with $w=0.1$ eV, mode D is still stiff at the zone center. In comparison, the energy change corresponding to mode C has a very flat landscape. The inset in Fig. 6(a) is a zoom-in view of the details for mode C. We see that the $\alpha=0$ point is actually a local maximum, which means that the phonon displacement can bring the tube to a slightly lower energy configuration. This result corroborates well with the phonon dispersion result in Fig. 3 that with $w=0.1$ eV, mode C at $k=0$ is soft.

We show in Fig. 6(b) the frozen phonon results calculated with a smaller Fermi surface smearing of $w=0.025$ eV. The inset in Fig. 6(b) is an expanded view using a smaller energy scale. Again, dots and squares correspond, respectively, to the frozen phonon displacement of modes C and D at $q=0$, and the lines are the fourth order polynomial fits. It is interesting to note that lattice distortion according to the eigenvector of mode C at $q=0$ gives positive energy changes, which can be fitted very well with a parabola. This is consistent with the phonon dispersion results that at $w=0.025$ eV, mode C is unstable near the nesting q vector of $q=k_+—k_-=0.13\pi/a$, but it has a positive frequency at the zone center. For frozen phonon displacements of mode D, the $\alpha=0$ point is a local maximum, consistent with the phonon dispersion results that the zone center mode of branch D has imaginary frequencies.

D. Model to explain the behavior

In order to gain a better understanding of the evolution of the phonon instabilities as shown in Figs. 2–4, we employ a model that describes the renormalization of an Einstein-like phonon with a bare frequency Ω_0 due to the coupling to two electronic bands. The renormalized frequencies are given by

$$\omega^2(q) = \Omega_0^2 + \sum_{n,n'} G_{n,n'} \chi_{n,n'}(q),$$

where n is 1 or 2, with $n=1$ standing for the negative mass band, and $n=2$ for the positive mass band. The susceptibility functions

$$\chi_{n,n'}(q) = \frac{1}{N_k} \sum_k \frac{f(e_{k,n}) - f(e_{k+q,n'})}{e_{k,n} - e_{k+q,n'}}$$

are evaluated using a two-band model, where the dispersion of the two LDA electronic bands crossing the Fermi energy are approximated by quadratic functions that reproduce the energies at $k=0$ and the k values at the Fermi-level crossings. The Gaussian broadening functions are denoted by $f(e)$. The $G_{n,n'}$ are the coupling constants that are taken to be independent of phonon or electron momenta. We will see that this

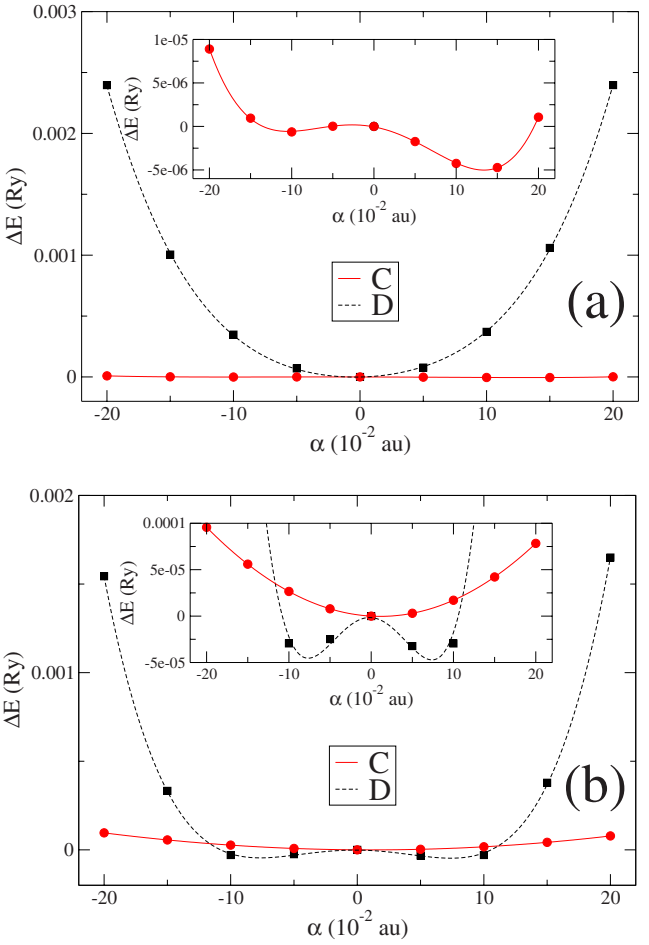

FIG. 6. (Color online) The energy changes when the lattice is distorted by frozen phonon displacements. Dots and squares correspond, respectively, to the frozen phonon displacements of modes C and D at zone center, and the lines are fourth order polynomial fits. The insets show expanded views near $\Delta E=0$. Results in Figs. 6(a) and 6(b) are calculated with Gaussian broadening widths of $w=0.1$ eV and of $w=0.025$ eV, respectively.

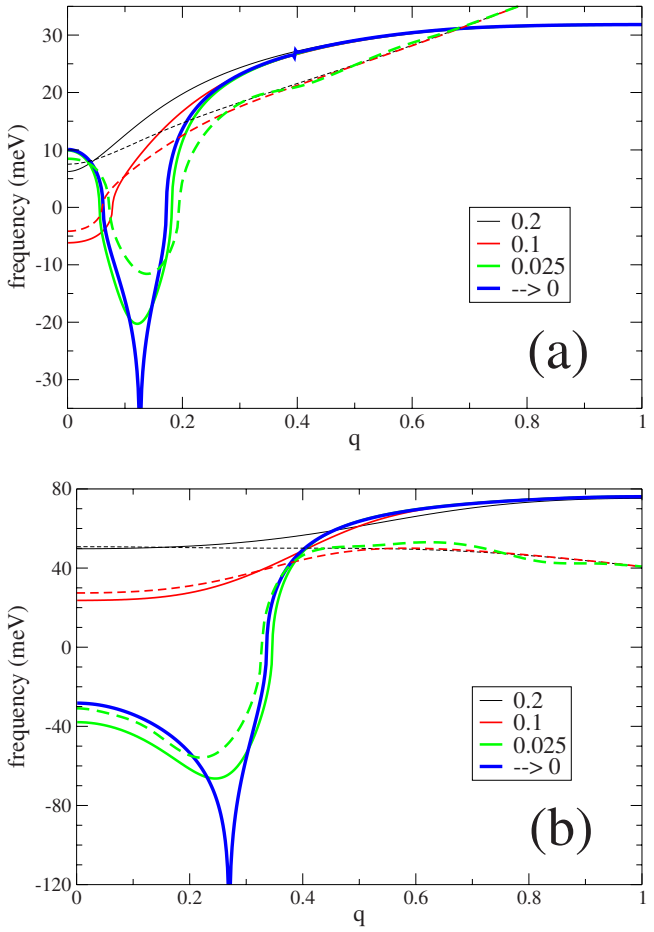

FIG. 7. (Color online) The solid lines show the phonon frequencies for a model that describes Einstein-like phonons with their bare frequency renormalized due to the coupling to two electronic bands. Different colors represent different smearing at the Fermi level, as labeled in the legend. The dotted lines are the phonon dispersion curves calculated from first principles. Figure 7(a) shows that the behavior of branch C is obtained when only the interband coupling is taken into account. Figure 7(b) shows that when only the intraband coupling of the negative mass band is nonzero, we get the behavior of branch D.

simple ansatz already gives the salient features of the phonon anomaly, which is due to the diverging behavior of the susceptibility. Typically, the k summation was performed with $N_k=10\,000$ k points.

As shown in Fig. 7, this simple two-band model is capable of describing the main features of the phonon instabilities for both branches C and D. The solid lines in Fig. 7(a) show the development of the phonon anomalies as the Fermi surface sharpens according to the model when only the interband coupling ($G_{12}=G_{21}$) is taken into account. The dotted lines are the phonon dispersion curves calculated from first principles. The important behaviors of branch C are captured by the simple model. In particular, the model gives the following features: (1) All frequencies are positive for a Fermi surface smearing of $w=0.2$ eV; (2) when $w=0.1$, a softening that leads to unstable modes for $q<0.1\pi/a$; (3) when $w=0.025$, modes become soft in the range $0.1\pi/a<q<0.2\pi/a$, but at $q=0$, the mode is stiffened and the frequency is positive again. Thus, all essential features of the first principles results are reproduced. It is not practical to go to an infinitely dense k point grid using first principles calculations, but we can follow the development of the phonon anomalies to the limit of zero smearing using the model. For very small smearing, the model finds that the susceptibility diverges at $q=0.13\pi/a$ and modes in the vicinity of $q=0$ remain stable.

When only the intraband coupling of the negative mass band (G_{11}) is nonzero, we get the behavior of branch D as shown in Fig. 7(b): (1) All frequencies are positive for $w=0.2$ eV; (2) a softening is found for $w=0.1$ eV especially near $q=0$, but all frequencies remain positive; (3) for $w=0.025$ eV all phonons with $q<0.35\pi/a$ become soft, with a valley at $q=0.26\pi/a$. Again, we can use the model to visualize the zero Fermi surface smearing limits. For very small broadening, the model predicts a singularity at $0.26\pi/a$, but the range of unstable phonons extends to the zone center.

E. Full relaxation within the constraint of primitive unit cell

We note that the phonon dispersions shown in Fig. 4 indicate that the system is unstable. However, the ground state atomic structure cannot be predicted by the phonon calculations. It would be interesting to know whether the lowest energy structure is related to the eigenvectors of the soft modes. Since the softest modes are at a finite q vector, the corresponding supercell would be too large for a search for the ground state geometry. We worked with the primitive unit cell and attempted to search for the lowest energy structure within the constraint of 20 atoms/cell and a small Gaussian broadening. We found that the lowest energy structure at $q=0$ is just about 1 mRy/unit cell lower than undistorted structure, and in addition, the distortion is essentially a linear combination of the phonon eigenvectors of branches C and D at the zone center. The amplitude of mode C is about five times larger than that of mode D, which is consistent with the frozen phonon results shown in Fig. 6 that shows that distortion according to mode C causes little change in energy. Since the eigenvector of mode C at the zone center corresponds to an elliptical distortion, the cross section of the tube becomes slightly elliptical, and the reduced symmetry opens a small gap near the Fermi level. The results are similar to those obtained in Ref. 4. The symmetry breaking and the resulting gap opening accounts for the energy gain. We have also tried to search for the minimum in the space of the generalized-coordinates defined by the eigenvectors of modes C and D, and the minimum point is basically the same as we found from direct relaxation. So, we found that the normal coordinates of the soft phonons do give us some useful information about the ground state atomic structure for $q=0$. It is of course difficult to speculate whether the true ground state can be described entirely as a linear combination of the softest modes shown in Fig. 4 at finite q vectors.

IV. SUMMARY

Most of the modes, including the acoustic modes, are hardly affected by the change of the Fermi surface smearing

in the range of 0.2–0.025 eV. Two phonon branches, labeled *C* and *D*, are strongly renormalized. The branch *D* shows a monotonic decrease in frequency near the region of small q vectors, and a $q=0.26\pi/a$ anomaly develops gradually due to intraband nesting. At $w=0.025$ eV, the phonon anomaly is fully manifested in the phonon dispersion and a whole range of wave vectors becomes soft near $q=0.26\pi/a$, extending all the way to the zone center. The development of the anomaly for the branch *C* is more complex, showing soft mode near the zone center first at $w=0.1$ eV. When Fermi surface smearing is reduced to $w=0.025$ eV, the modes near $q=0.13\pi/a$ become soft, driven by the interband nesting. However, the mode at zone center becomes stable again. The distortion of the fully relaxed structure at the zone center (for small Fermi surface smearing) is found to be essentially a linear combination of the soft modes *C* and *D* at zone center.

ACKNOWLEDGMENTS

We thank Y. J. Feng for assistance in the calculations. Research work in Hong Kong was supported by RPC06/07.SC21. The mutual visits were supported by the DAAD-HK travel grant D/05/06872 (G_HK022/05-II).

[1] Z. K. Tang, H. D. Sun, J. Wang, J. S. Chen, and G. D. Li, Appl. Phys. Lett. **73**, 2287 (1998); N. Wang, Z. K. Tang, G. D. Li, and J. S. Chen, Nature (London) **408**, 50 (2000).

[2] H. J. Liu and C. T. Chan, Phys. Rev. B **66**, 115416 (2002); M. Machon, S. Reich, C. Thomsen, D. Sanchez-Portal, and P. Ordejon, *ibid.* **66**, 155410 (2002).

[3] K.-P. Bohnen, R. Heid, H. J. Liu, and C. T. Chan, Phys. Rev. Lett. **93**, 245501 (2004).

[4] D. Connetable, G.-M. Rignanese, J.-C. Charlier, and X. Blasè, Phys. Rev. Lett. **94**, 015503 (2005).

[5] R. Barnett, E. Demler, and E. Kaxiras, Phys. Rev. B **71**, 035429 (2005).

[6] S. Baroni, P. Giannozzi, and A. Testa, Phys. Rev. Lett. **58**, 1861 (1987).

[7] B. Meyer, C. Elsässer, and M. Fähnle, FORTRAN90 Program for Mixed-Basis Pseudopotential Calculations for Crystals, Max-Planck-Institut für Metallforschung, Stuttgart (unpublished).

[8] J. R. Chelikowsky and S. G. Louie, Phys. Rev. B **29**, 3470 (1984).

[9] R. Heid and K.-P. Bohnen, Phys. Rev. B **60**, R3709 (1999).

[10] C. L. Fu and K. M. Ho, Phys. Rev. B **28**, 5480 (1983).

[11] X. Blasè, L. X. Benedict, E. L. Shirley, and S. G. Louie, Phys. Rev. Lett. **72**, 1878 (1994).

[12] W. S. Su, T. C. Leung, B. Li, and C. T. Chan, Appl. Phys. Lett. **90**, 163103 (2007).

[13] H. J. Liu and C. T. Chan, Solid State Commun. **125**, 77 (2003).

[14] S. Piscanec, M. Lazzeri, J. Robertson, A. C. Ferrari, and F. Mauri, Phys. Rev. B **75**, 035427 (2007).

[15] S. V. Goupalov, Phys. Rev. B **71**, 085420 (2005).